Tunnelling and Underground Space Technology 85 (2019) 1–11

Contents lists available at ScienceDirect

Tunnelling and Underground Space Technology

journal homepage: www.elsevier.com/locate/tust

An impact imaging method for monitoring on construction of immersed tube tunnel foundation treated by sand-filling method

Ailan Che*, Renjie Zhu, Yanmin Fan, Shaokong Feng

School of Naval Architecture, Ocean and Civil Engineering, Shanghai Jiaotong University, 800 Dongchuan-Road, Shanghai 200240, China

ARTICLE INFO

Keywords:
Immersed tube tunnel
P-wave impact imaging method (PII)
Real-time monitoring
Full scale model test
Sand-filling method

ABSTRACT

Sand filling method (sand-flow method) is widely used in the treatment of immersed tube tunnel foundation, but quick and reliable method for real-time monitoring on the formation of sand-deposit and the connection of sand-deposit between neighboring sand filling hole is absent. In this paper, a full-scale model of immersed tube tunnel foundation treated by sand filling method was conducted. The case was simplified as a multi-layered media problem, and a nondestructive testing method based on P-wave was explored to control the sand filling time in different hole. Through model testing, the relationship between the change rate of P-wave response energy and the radius of the sand-deposit is established. Kriging interpolation principle was employed to make a complete evaluation of the sand-deposit. The radius of sand-deposit measured by the P-wave impact imaging method (PII) agree well with the average radius observed by the observation window. Comparing the results of PII in sand filling hole with the relative compactedness of sand foundation after the sand filling, it can be found that the sand foundation boundary detected by PII method agree well with model test result, and the region with higher relative compactedness has a good correspondence with the regions with high change rate of PII. So, the PII method can detect the radius and the distribution of relative compactedness of sand-deposit. Because the method is convenient in calculation, the construction of sand filling foundation can be monitored in real time by PII method. In conclusion, the method can be used to monitor sand-filling treatment in immersed tube tunnel on real-time, and provide a scientific basis for the design and construction of immersed tube tunnel Engineering.

1. Introduction

In China, with the rapid development of economy and society, the construction of traffic facilities across waters grows quickly. Immersed-tube tunnel, which has looser requirements on hydrogeological conditions, simple construction equipment, high utilization rate of cross-section, is widely used in underwater tunnel for crossing river and strait (Glerum, 1995; Rasmussen, 1997). Sand filling method is an important method for foundation treatment of immersed tube tunnel. In this method, mixture of sand-water is injected into the foundation layer through sand filling hole, as is shown in Fig. 2 (Wang et al., 2009). Sand filling method was first applied in Vlake Tunnel of Holland in 1978 (Tongeren and Van, 1978), and it has been developed in Sydney Harbour Tunnel (Gomes, 1991), Guangzhou Pearl River immersed tube tunnel, Shanghai outer ring immersed tube tunnel (Pan et al., 2004), Guangzhou Chau Tau Tsui immersed tube tunnel (Wei et al., 2014) and Guangzhou Biological Island-University City Tunnel (Wang et al., 2009). However, a lot of complex engineering problems have arisen in this process. Grantz (2001a, 2001b) stated that the treatment of foundation plays an important role in the settlement of immersed tube tunnel, and the treatment process is difficult to forecast and control. Zhang and Gao (2003) concluded that the uneven of foundation will cause un-uniform settlement or local cracking of tube. Therefore, in the process of sand flowing, the expansion of sand-deposit and the distribution of relative compactedness must be monitored in real-time to ensure the quality of treatment.

The traditional methods used in monitoring sand filling treatment is empirical, and they focus on monitoring of overall settlement. For example, Chen et al. (2002) established the empirical relationship between the pressure of sand filling and the extension radius of sand-deposit through the model test of immersed tube foundation. Wei et al. (2014) created a real-time sand-deposit detector in model test to monitor the expansion of sand tray. But the detector will destroy the water resistance of immersed tubes. In practice, engineers often let the diver touch the underwater to determine whether the sand filling is complete. So, the traditional method is impracticable to realize the real-time monitoring of sand-deposit expansion.

Recently, the implementation of elastic-wave-based nondestructive

* Corresponding author.
E-mail address: alche@sjtu.edu.cn (A. Che).

https://doi.org/10.1016/j.tust.2018.11.027
Received 11 April 2017; Received in revised form 17 August 2018; Accepted 24 November 2018

testing technologies has received significant attention in civil engineering. Traditional elastic-wave inspection methods recognize internal structure from changes in received signals using a single point source/point receiver arrangement (Malhotra and Carino, 1991). However, modern elastic-wave imaging techniques employ a multiple source/receiver arrangement to scan defects in structure (Liu et al., 1996). An elastic-wave-based imaging method is used to detect the tip off surface-breaking cracks in concrete, and the result shows that the point-source / point-receiver scheme is suitable for the inspection of on-site civil infrastructures (Chang et al., 2001; Tong et al., 2007).

With impact imaging method as context, layered structures are known as propagations of elastic wave. Elastic waves with long wave lengths have given elastic-wave inspection methods the potential for examination of layered structures. For example, Dalton found that guided elastic waves can localize damage sensitively (Dalton et al., 2001). With guided elastic waves Rose has supplied an extremely comprehensive account of the state of the art (Rose, 2002). P-waves capable of travelling through liquids have given P-wave imaging method considerable potential for the observation of layered structures with liquid interlayer. Che et al. proposed an elastic-wave imaging method for the investigation of the grouting construction of immersed tube tunnels (Che et al., 2011; Feng et al., 2013; Liu et al., 2013). This method could be a practical and effective one for the inspection of structure in civil infrastructures. However, these studies focus on a single scale and time-consuming.

Nanchang Honggu immersed tube tunnel in China is taken as background; precede a full-scale model test with sand filling method. We proposed a real-time monitoring method based on P-wave response energy, and it can be implemented in the observation of layered structures with liquid interlayer. The method was applied in the model testing. The relationship between the variation of P-wave response energy and the radius of sand-deposit was gained. Furthermore, Kriging interpolation principle was used to describe the spatial and temporal evolution of sand - flow foundation. The research results can provide reference for the use of sand filling method, and the design and construction of immerged tunnel.

2. P-wave impact imaging method

2.1. Principles

In layered structure, elastic wave will be reflected and refracted on the interface when it travels through an interface between two layers with different properties. The reflected wave contains P-wave, SV-wave and Rayleigh wave, caused by difficult refraction, reflex and superposition happened in different mediums, all of which should satisfy wave equation. In this paper, the layered structure was simplified into multiple thin layered media. The top concrete layer is considered as a thin layer. The sand filling layer is considered as a variable layer. The plain concrete layer and rubbler cushion layer are considered as foundation layers. The parameters of the foundation layers can be considered unchangeable. In addition, the wave energy has already attenuated when it spreads to the foundation layers. The influence of the foundation layers on reflected wave is very small. Vertical P-wave was using as excitation wave. The interface reflection behavior of elastic wave between two layers will be firstly discussed, and then the influence caused by interface reflection on the top of thin layer will be taken into further discussion.

Fig. 1(a) shows the P-wave propagation at an interface between two different materials. ρ_i (i = 1,2) is the mass density associated to media i; $V_{p,i}$ denote the wave velocity of P-wave in media. It makes easier to calculate the reflection coefficient without considering the influence of converted wave. When the plane P-wave incidents onto the interface vertically between two different materials, there exists the reflection of P-wave in media 1. The reflection coefficient R_p can be expressed as:

$$R_p = \frac{A_2}{A_1} = \frac{\rho_2 V_{p,2} - \rho_1 V_{p,1}}{\rho_2 V_{p,2} + \rho_1 V_{p,1}} \tag{1}$$

while A_1 and A_2 denote the amplitude of incident P-wave and reflected P-wave in media 1, separately.

Further investigation on the result caused by upper thin layer will be demonstrated as follow. Fig. 1(b) shows the P-wave propagation in a structure with thin layer. The reflection and transmission in thin layer is the superposition result of single wave after thousands times of reflection and transmission. Each single wave interference was caused due to thin layer and the property of layers. Take vertical incidence of P-wave into thin layer as an example. The upper and bottom boundary is called r_1, r_2, the wave velocity of P-wave in this three kinds of media is $V_{p,1}$, $V_{p,2}$, $V_{p,3}$, the impedance of P-wave is Z_1, Z_2, Z_3, the thinness of thin layer is Δh.

After wave equation derived, the ratio of every two adjacent reflection waves in the thin-layer reflection under the vertical incidence of P wave can be obtained.

$$\begin{aligned}
&\delta = \frac{A_{p1221}}{A_{p11}} = \frac{t_1' r_2 t_1 A_{p1}}{r_1 A_{p1}} = \frac{4Z_1 Z_2 (Z_3 - Z_2)}{(Z_2 - Z_1)(Z_1 + Z_2)(Z_2 + Z_3)} \\
&r_1 = \frac{A_{p11}}{A_{p1}} = \frac{Z_2 - Z_1}{Z_2 + Z_1}, \quad t_1 = \frac{A_{p12}}{A_{p1}} = \frac{2Z_1}{Z_2 + Z_1} \\
&r_2 = \frac{A_{p122}}{A_{p12}} = \frac{Z_3 - Z_2}{Z_3 + Z_2}, \quad t_1' = \frac{A_{p1221}}{A_{p122}} = \frac{2Z_2}{Z_2 + Z_1} \\
&\frac{A_{p122221}}{A_{p1221}} = \frac{A_{p1222221}}{A_{p122221}} = \cdots = b = \frac{(Z_1 - Z_2)(Z_3 - Z_2)}{(Z_2 + Z_1)(Z_3 + Z_2)}
\end{aligned} \tag{2}$$

Reflection wave P_{11}' in media I is the result of superposition of all multiple reflection waves. Currently, $\Delta h \leqslant v_2$, therefore:

$$\begin{aligned}
&u_{p_{11}'}(z) = (A_{p_{11}} + A_{p_{1221}} + A_{p_{122221}} + A_{p_{12222221}} + A_{p_{1222222221}}) \exp\left[i2\pi f\left(t + \frac{z}{v_1}\right)\right] \\
&= (1 + \delta + b + b^2 + b^3) A_{p_{11}} \exp[i2\pi f (t + \tfrac{z}{v_1})] \\
&= (1 + \delta + b + b^2 + b^3) u_{p11}
\end{aligned} \tag{3}$$

In layered medium with thick layer and thin layer, superposition effect was caused by the reflection and transmission of thin layer media. But if only the first layer of the model is thin layer, it is enough to multiply corresponding coefficient in the calculation of structural reflection coefficient. Which means the thin layer will improve the sensitivity of the monitoring system.

We proposed the change rate of P-wave response energy (D_i), and it can be calculated by the following equation:

$$D_i = 1 - \frac{P_i}{P_0} \tag{4}$$

While P_0 represent the response energy of the monitoring points before sand filling; P_i (i = 1, 2, …, n) represent the average absolute value of the P-wave amplitudes on each monitoring point. And the number of acquisitions is represented in the sand filling process. From the above Equations, reflection coefficient is related to physical properties of the tests material. And it can also be determined from the amplitudes of the incident and the reflected wave. Consequently, D_i can describe the amount of wave energy. It is possible to establish a relationship between D_i and a certain mechanical parameter of the test material.

2.2. Detection process and data processing

In this paper, the distance between the sand filling hole and the out edge of the sand-deposit which contact the bottom surface of the test platform is defined as the sand-deposit radius, as shown in Fig. 2. To match the PII measuring scheme in civil engineering, the monitoring is managed with a point-source/point-receiver set with a specified space (Δx). Δx is much smaller than Δh (the thickness of the structure). Therefore, incident wave can be simplified into vertical P-wave.

A series of impact-and-receive operations are performed on the

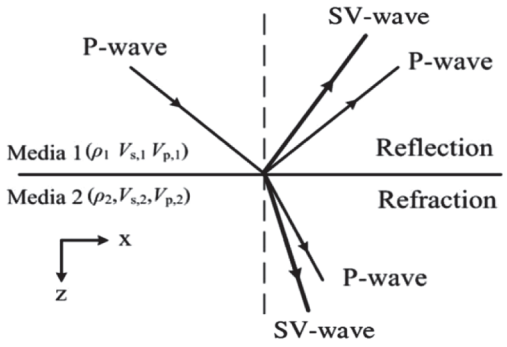

(a) P-wave propagation at an interface

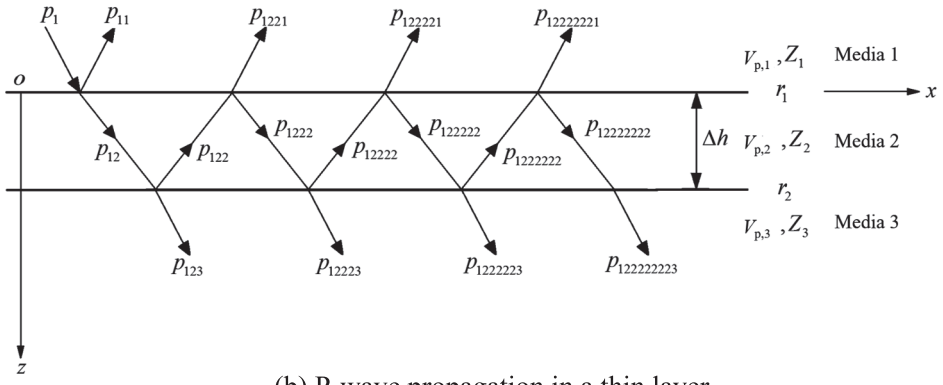

(b) P-wave propagation in a thin layer

Fig. 1. Characteristics of P-wave propagation.

surface of test platform in sequence with an interval of Δd, as shown in Fig. 2. The locations of a set of the source and receiver for the i-th measurement are represented by S_i and R_i separately. Furthermore, let $T_i(t)$ be the response signal recorded at R_i for this measurement.

The processing of PII data processing mainly includes three parts:

(1) Waveform processing: Assign the positions of source and receiver to the seismic data at the beginning of data processing. Normalize the seismic data ($T_i(t)$) with the acceleration (S_i) recorded by an accelerometer on the hammer to reduce the influence of the variation of impact strength. Abstract common offset traces from the field of common source data to create a common offset gather. The data may present different types of noise. Reduce noise with time windows and band pass filters. Reorder the traces in the common offset gather according to their position (R_i) on the survey line to create a Time-Waveform section. All further processing will be conducted on this section.

(2) Calculation of the response energy: The average absolute value of the P-wave amplitudes is defined as the response energy on each monitoring point, which we shall denote by P_i (i = 1, 2, …, n). 'i' represents the number of acquisitions in the sand filling process. The impact response can be represented as a line graph.

(3) Imaging processing: The change rate of response energy (D_i) can be calculated by Eq. (4). Based on the numerical results of imaging processing, kriging interpolation method is used to obtain the cloud map of D_i, and the construction situation of the foundation layer is monitoring in real time.

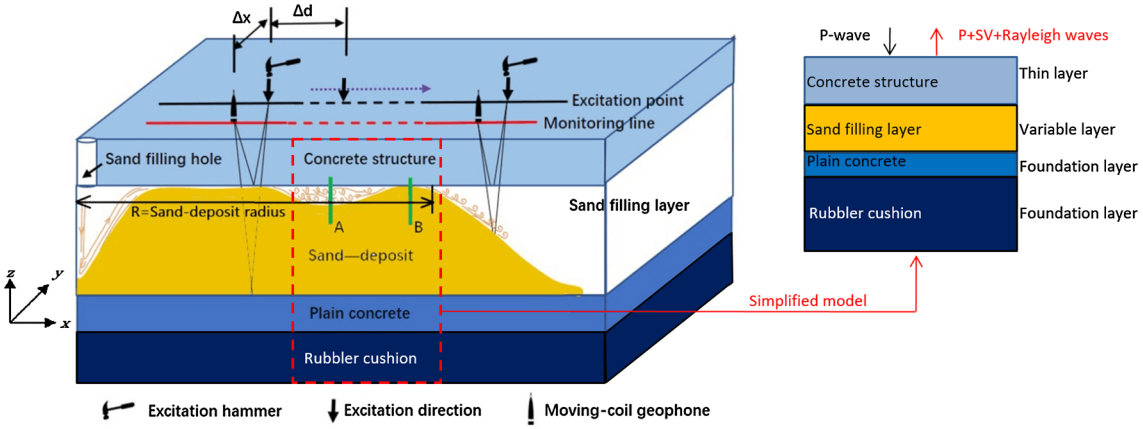

Fig. 2. Schematic diagram.

3. Model test system

The design of the model test system is based on Nanchang Honggu immersed tube tunnel, which is 329 m long. The tunnel foundation is treated by sand-flow method. The length and width of the bottom of the immersed tube is much larger than the thickness, so it is reasonable to simplify the model into a multi-layered media problem. In this search, the model system consists of two parts: Model system of immersed tunnel and sand-injection system are the responsible part for simulating sand filling process of immersed tunnel; measurement system is that part for monitor ing the construction of sand foundation. In this part, P-wave impact imaging method was utilized, and observation window was used to verify the measurement results of PII.

3.1. Model system of immersed tunnel and sand-injection system

3.1.1. Model system of immersed tunnel

The model consists of two parts: an experimental tank and a testing platform. The testing platform with a dimension of 25 m × 23.5 (length × width) is made of reinforced concrete, and it is used to simulate immersed tube and to perform test data acquisitions, as shown in Fig. 3. There are four sand filling holes in the test platform, and the filling sequence is A, B, C, and D.

The dimension of experimental tank is 30 m × 27.5 m (length × width). The bottom of the tank is paved with 0.2 m gravel cushion and 0.1 m concrete cushion, and the water depth in the tank is 1 m. The testing platform in the experimental tank was supported by concrete pole which are 0.6 m × 0.5 m × 0.5 m (height × length × width), and the thickness of sand filling layer is 0.6 m, as is shown in Fig. 3.

The sand used in the test with a density of 1500 kg/m^3, and repose angle of 31°, is the same material as the foundation treatment design of Honggu tunnel in Nanchang. Since the ratio of sand to water is 1: 9 has been proved to be appropriate in the experience of engineering practice (Chen et al., 2002), the simulated material for model testing was developed.

3.1.2. Sand-injection system

The sand-injection system includes five parts: sand mixer, water-sand mixing tank, sand pump, water-sand conveyance part and pressure controller part. Sand mixer was used to supply uniform particle distribution sand to sand–water mixing tank. The sand pump was used to pump sand–water mixer from mixing tank, and inject the high-pressure sand–water mixture to sand filling layer through water-sand conveyance part. All the equipment has the same parameters as construction equipment in sand filling method. The photos of test equipment system are shown in Fig. 4.

According to the design of Nanchang Honggu immersed tube tunnel, sand is injected into sand–water mixing tank through conveyor belt. Water is pumped into sand–water mixer from experimental tank by water pump. After fully mixed, the sand–water mixture was drawn and pumped into sand-filling layer by sand-injection system. The sediment of sand particles formed sand deposit and the water pumped into sand-water mixing tank.

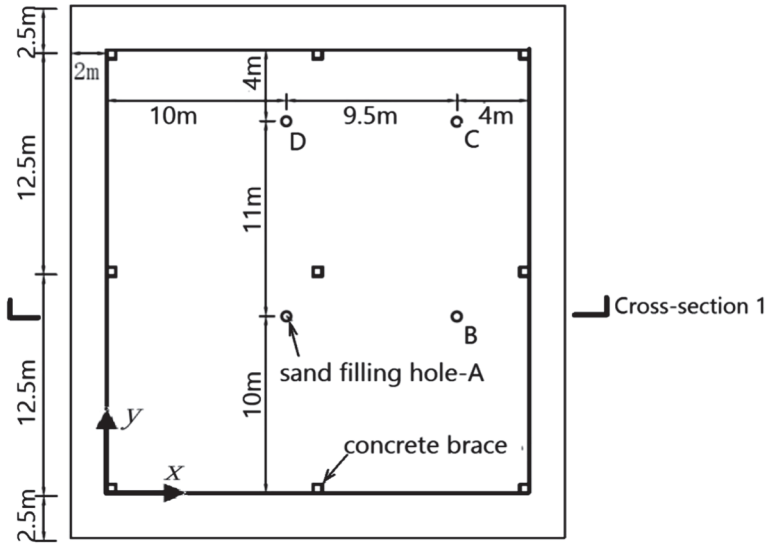

(a) Floor plan of testing model

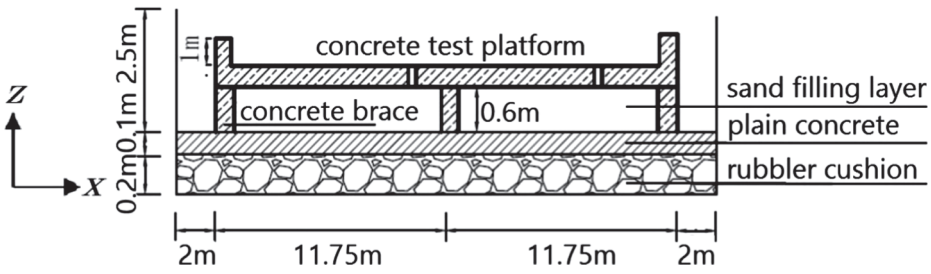

(b) Sectional view of testing model (Cross-section 1)

Fig. 3. Full - size testing model of immersed tube tunnel (cross-section).

① Sand mixer ② Water-sand mixing tank ③ Pressure controller part

④ Sand pump ⑤ Water-sand conveyance part

Fig. 4. Sand-injection system.

(a) Hammer (b) Receiver (c) Seismograph (d) Monitoring line

Fig. 5. Equipment for monitoring work in field.

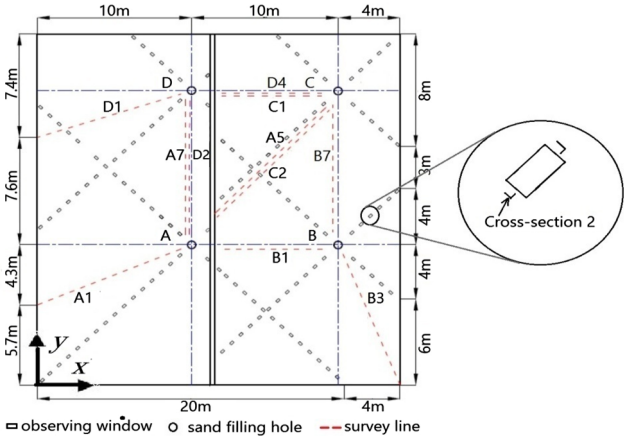

Fig. 6. Position of observation window and monitoring line.

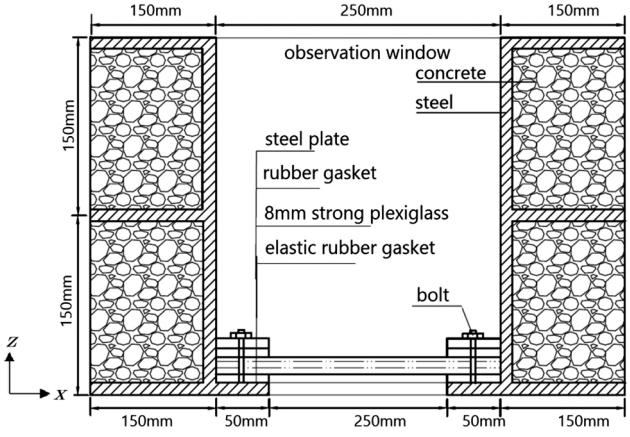

Fig. 7. Sectional view of observation window (Cross-section 2).

The foundation is constructed in this order: the middle and then the side. So, the filling sequence is A, D, C, and B. The time of sand filling in different hole is controlled by designed radius of sand deposit and interface width of adjacent sand deposit. The designed radius of A and D is 8 m, B and C is 4.5 m. The interface width of A and D is 16 m, D and C is 12 m, C and B is 12 m, B and A is 8 m. The radius is detected by measurement system, and interface width is monitored by P-wave impact imaging method.

3.2. Measurement system

In this research, observation window was designed to verify the correctness of PII method. PII method is applied in the process of sand filling. The shape and distribution of relative compactedness of sand foundation were investigated after sand-filling. In this paper, the distance between the monitoring point and the sand filling hole is defined as the monitoring distance.

3.2.1. P-wave impact imaging method

The monitoring equipment of P-wave impact imaging method

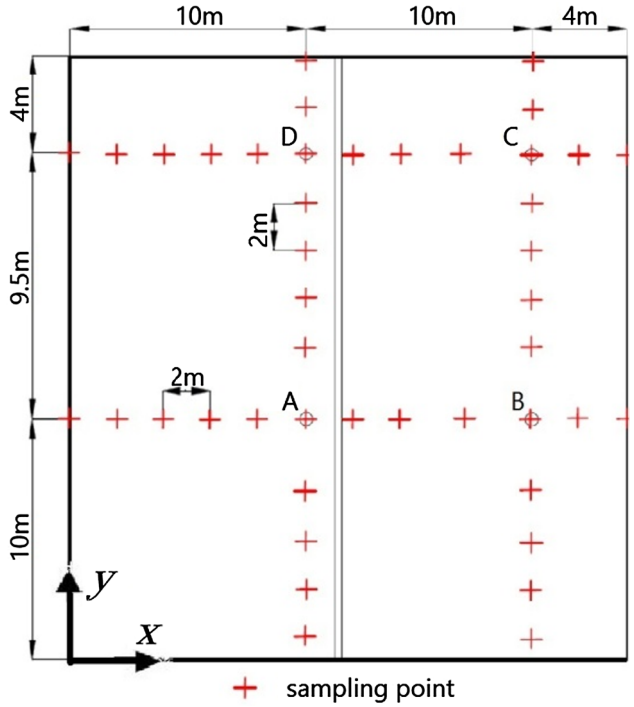

Fig. 8. Location of sampling points.

consist of three parts: signal excitation equipment (hammer), signal acquisition equipment (receiver, seismograph), and signal processing equipment, as shown in Fig. 5.

The impact signal excitation part composed of Trigger and hammer (250 g weight). It was used to generate the signal and record the excitation wave. When impacting the bottom of the immersed tube with the hammer, a P-wave is excited. The main frequency of the excitation wave is about 1000–1500 Hz. The signal acquisition equipment part comprised moving-coil geophone of vertical speed, which natural frequency is 200 Hz, and Geode digital seismic recorder, which is used to collect and store data. The signal processing equipment part was made up of computer, seismic wave analysis program and image processing program. It was used to analysis the characteristics of response P-wave and data imaging processing. The monitoring lines (length: 2.1–13.9 m) are arranged around the sand filling hole, as shown in Fig. 6.

The detector is arranged at 0.25 m interval on monitoring line, and the steel hammer is vertically excited at 0.25 m from the measuring point. The excitation energy is the controlled by the drop height of hammer.

3.2.2. Observation window

To verify the measurement results of PII, observation window was developed to measure the radius of sand-deposit during the sand filling, and the sketch of its structure is shown in Fig. 7.

The observation window was embedded at the construction process of the testing platform. And it is evenly distributed on two perpendicular intersecting lines. The intersection is the sand filling hole, as is

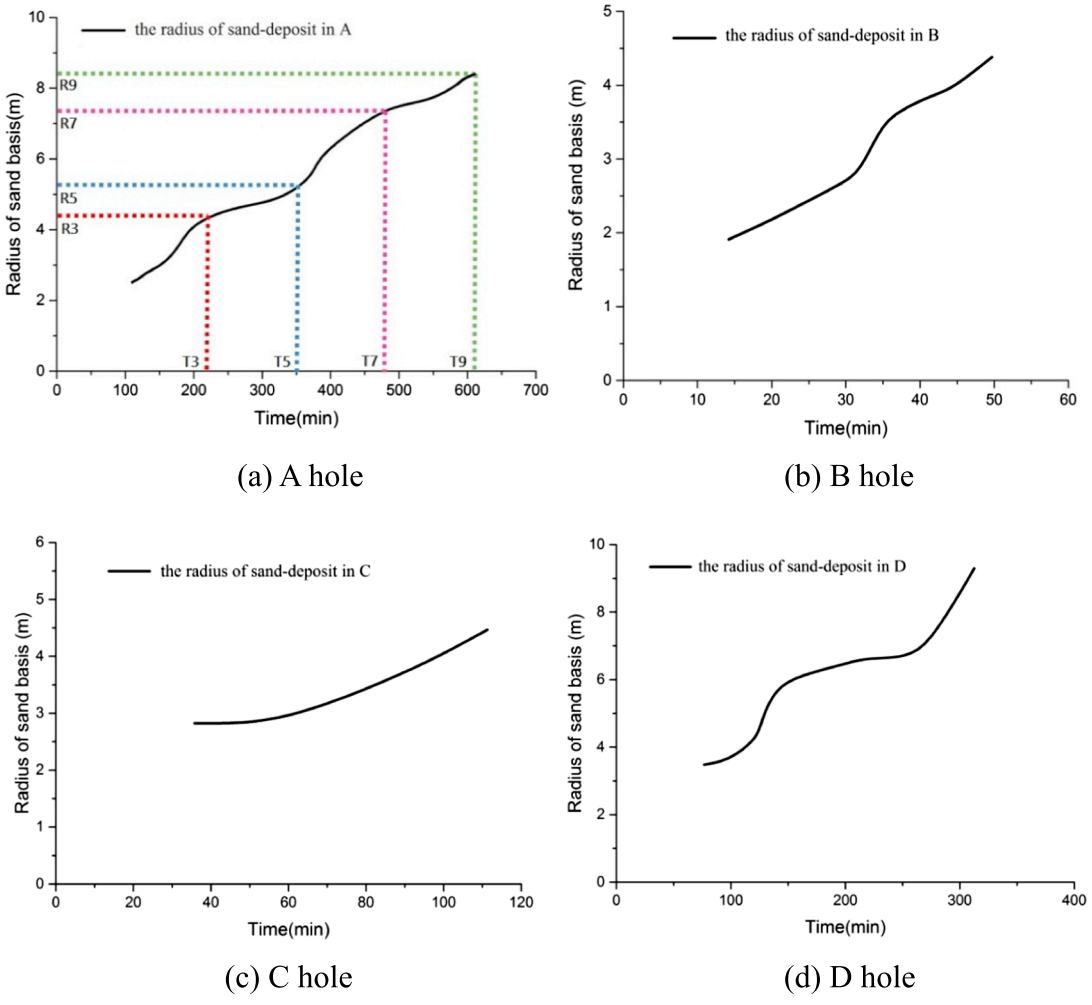

Fig. 9. Relationship of the radius of sand-deposit and time.

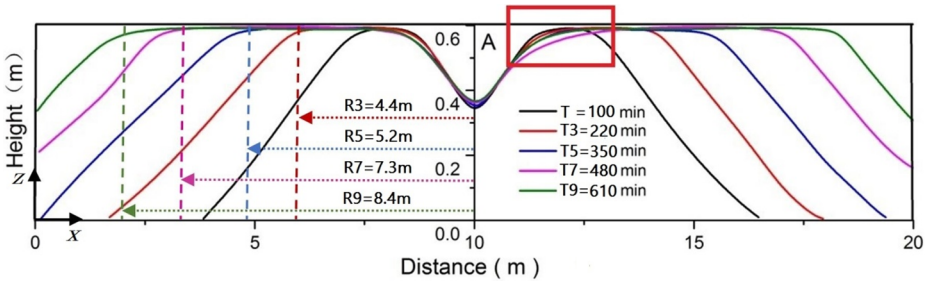

Fig. 10. Sketch of sand-deposit profiles in A hole.

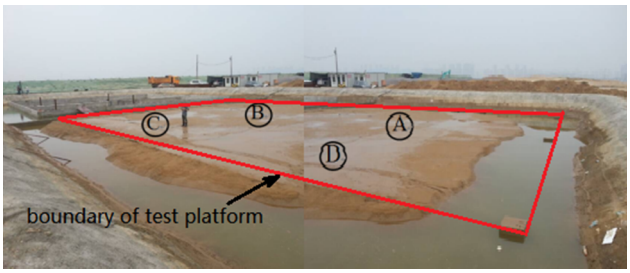

Fig. 11. Sand foundation after sand filling.

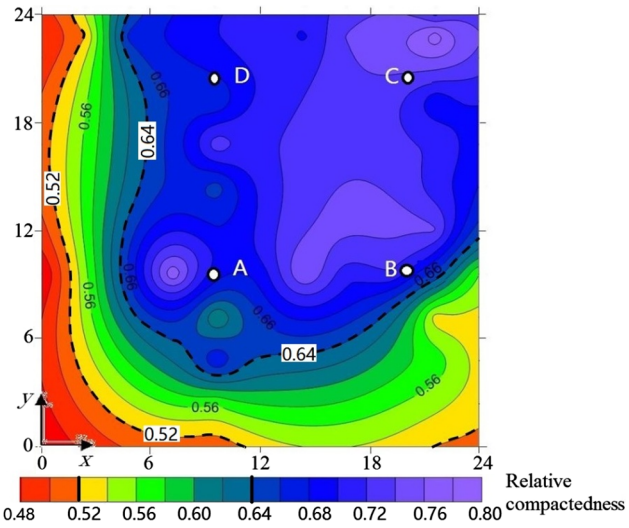

Fig. 12. Distribution of relative compactedness after sand filling.

shown in Fig. 6.

3.2.3. Test scheme and procedures

In the process of sand filling, the test data collection consists of three parts: using the observation window to record the expansion radius of sand-deposition, data collection of PII and the final relative compactedness of the filling-sand foundation. In the observation window, when sand do not migrate, the sand-deposition has been extended to the observation window in this direction, and the position of the observation window and observing time should be recorded. The P-wave impact imaging method detecting interval is 65 min, start with sand fill. The data recording interval is 50 μs, the recording length is 0.256 s, and the number of tracks is 2(2 × 1). Hammer-induced vibration is received by the speed detector and sent to the digital seismic recorder to generate the data file. To get the relative compactedness of the filling-sand foundation, we pumped water from the experimental tank after sand filling, and carried out stratified sampling at different positions of the foundation. The location of sampling points is shown in Fig. 8.

4. Test results and analysis

4.1. Results of observation window and compactedness of sand foundation

4.1.1. Results of observation window

During the experiment, we can record the average expansion of the sand-deposit radius near the A, B, C, D sand filling holes through the observation window. Fig. 9 shows the relationship between the radius of sand-deposit and sand filling time.

Fig. 9 indicates that the increasing speed of sand-deposits radius in different holes shows a trend that first increased and then decreased. The expansion speed of sand-deposit radius near A and D are faster than that near B and C. The reason is that the sand filling sequence of B and C is later than A and D, and the sand-deposit of B and C require less filling sand than A and D.

Fig. 9 shows the sketch of sand-deposit profiles of A sand filling hole. Fig. 9(a) and 10 show that the expansion speed of sand-deposit is slowly at the beginning of sand filling. When the sand-deposit radius accumulates to a certain degree, the radius increases quickly. But with the increase of sand-deposit radius, the transport channel of sand-water mixture decrease, so the expansion speed will decrease (Wei et al., 2014). Under the sand filling hole the sand-deposit has an impact pits about 1.8 m radius which was a result of high pressure mixture impingement. The interface of sand-deposit and test platform is constantly changing, and the part that is in contact may be separated by the scouring of sand-water mixture, as shown in the curve of 220 min in Fig. 10.

4.1.2. Result of the compactedness of sand foundation

After the sand filling, the test platform was removed and the water in the test tank is drawn out. We can get the shape of sand-deposit after sand filling, as shown in Fig. 11.

It can be noticed that the sand-deposit in different sand filling hole were expanded to the designed radius, and the intersection of adjacent sand deposit was filled well. The sand-deposit of B, C holes have been extended to the edge of the test platform, the sand-deposit of holes A and D did not extend to the boundary of test platform.

In Fig. 12, the portion of sand-deposit having a relative compactedness less than 0.52 is separate from the bottom face of test platform. These portions are mainly distributed in the vicinity of x axis and y axis, as shown in Fig. 12. The portion with a relative compactedness more than 0.64 is high density section. The reason is that the sand-deposits of A and D hole have compacting effect on the formation of sand-deposit of B and C hole, so the relative compactedness of the latter is larger than the former.

4.2. Analysis of P-wave response energy

By comparing the value of P-wave response energy measured in 0 min (before sand filling),220 min (the third time), 350 min (the fifth time), 480 min (the seventh time), 610 min (the ninth time) in A hole, we can get the relationship between the average seismic amplitude and the monitoring distance, and it is shown in Fig. 13.

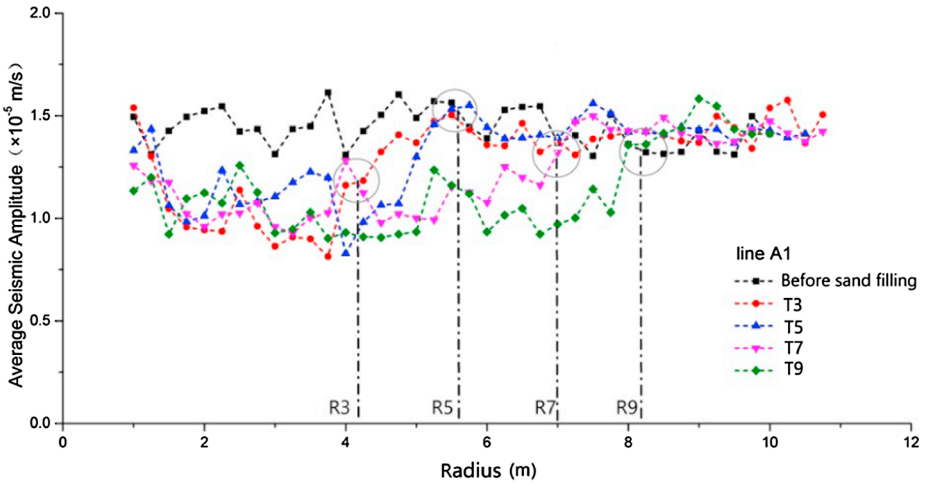

(a) monitoring line A1

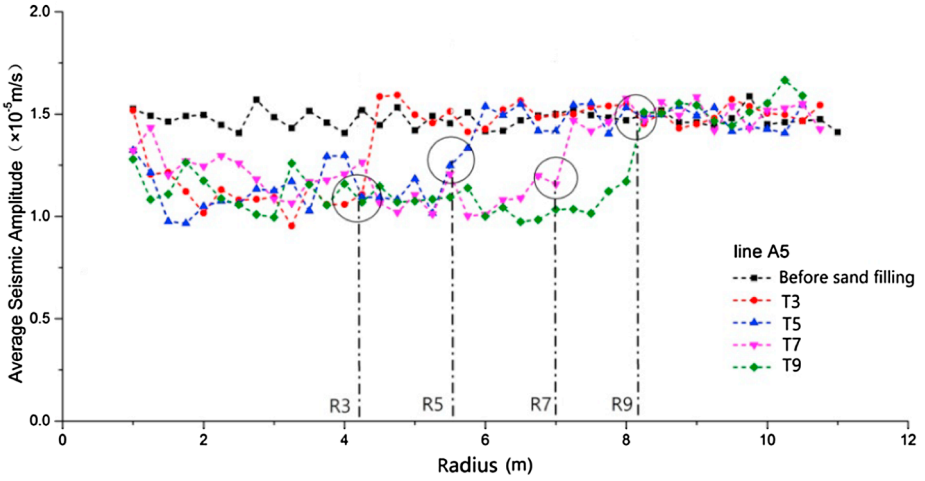

(b) monitoring line A5

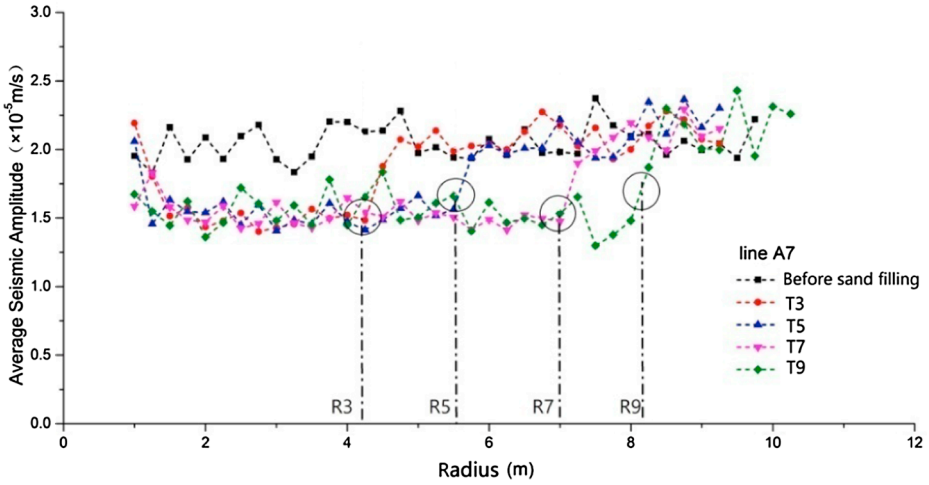

(c) monitoring line A7

Fig. 13. Relationship of average P-wave seismic amplitude and monitoring distance in A hole.

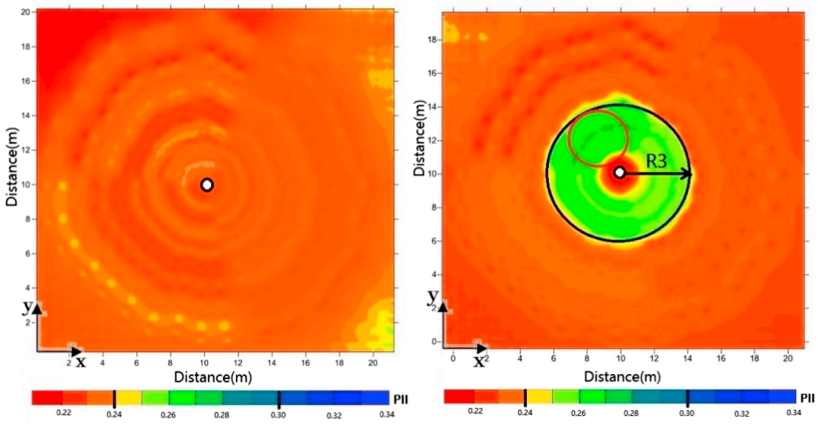

(a) Before sand filling(0 minutes) (b) The third measurement (220 minutes)

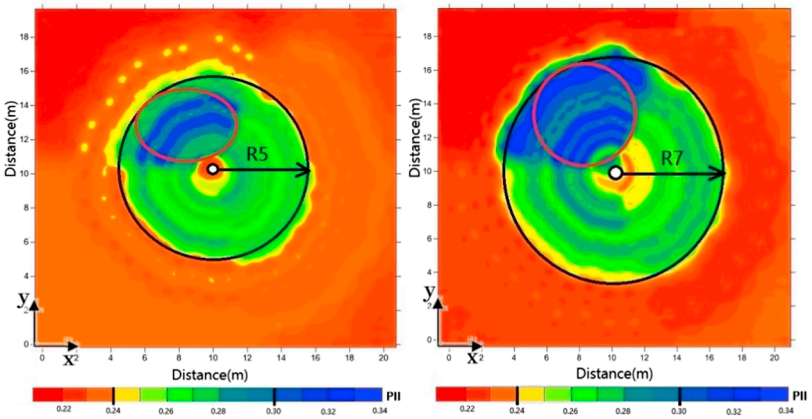

(c) The fifth measurement (350 minutes) (d) The seventh measurement (480 minutes)

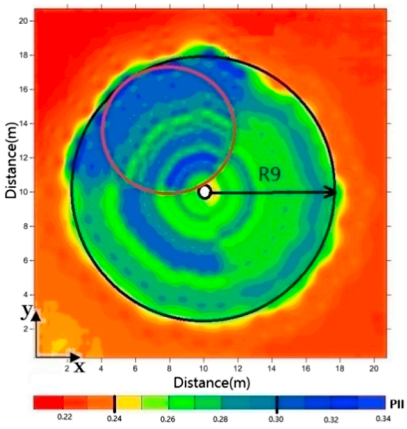

(e) The ninth measurement(610 minutes)

Fig. 14. Cloud map of the distribution of PII in hole A.

Firstly, by comparing (a), (b) and (c) in Fig. 13, we can find out that the maximum and minimum value of line A1 and A5 are consistent enough. It shows that the influence of observation windows on experimental results is very small. On the other hand, we found that the average seismic amplitudes before sand filling in (a) and (b) are 0.4–0.6 units lower than (c). The reason is that the different structure of testing platform in monitoring line A7 where near a beam structure caused the decrease of response energy. The monitoring distance of the broken lines a, b, c, and d is the radius of sand-deposit in 220 min, 350 min, 480 min and 610 min are measured by the observation window. In Fig. 13(a), (b) and (c), the mean average amplitudes at different locations before sand filling fluctuate around 1.5, 1.5 and 2.0 in a certain range. After the beginning of sand filling, with the increase of monitoring distance the curve of average seismic amplitude first decrease and fluctuate around a fixed value, and then increase and fluctuate around a larger fixed value. The monitoring distance value in the

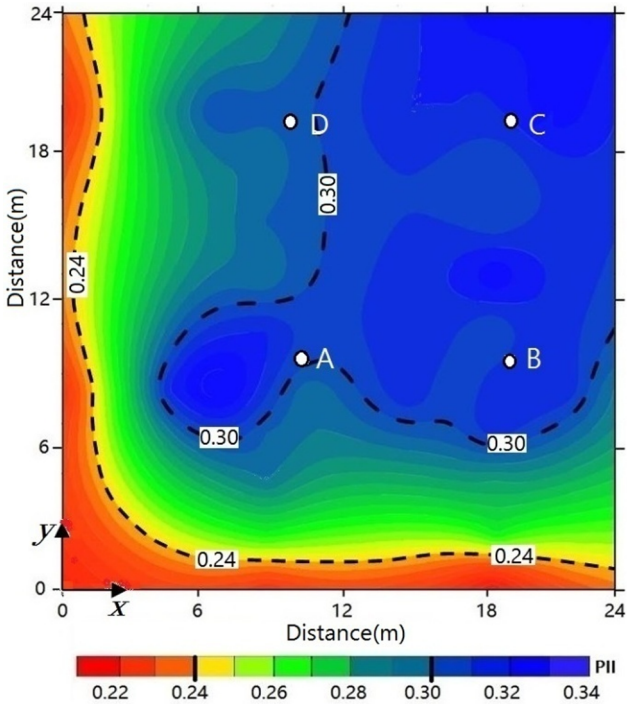

Fig. 15. Cloud map of PII.

position where the curve decrease is about 1.2 m which is the same as the radius of impact pit in sand-deposit. The position where the curve increase corresponds well to the position of a, b, c and d. The reason for this phenomenon is, when the sand-deposit contacts the bottom of the test platform, the mass density and the wave velocity of sand-deposit is significantly larger than those of water, so the reflection coefficient will decrease, as is shown in Eq. (3). So, it results in the change of the fluctuation range of average seismic amplitude value. Therefore, the radius of sand-deposit can be determined by the relationship line of average seismic amplitude and monitoring distance.

4.3. Results of P-wave impact imaging method

Based on the above chapter it can be found that the change rate of response energy is related to whether the bottom of test platform is in contact with the sand-deposit foundation. In order to conduct a complete evaluation of the sand-deposit, the change rate of response energy of each observed point is calculated by Eq. (4), and the effect of beam structure on testing platform is reduced according to the value at the same point on the observation line before sand filling. On the basis of the above analysis, by using Kriging interpolation method, we can get the real-time observation cloud of sand-deposit in hole A, as shown in Fig. 14. After sand filling, the cloud of PII in different hole will be got, as shown in Fig. 15.

Fig. 14 represents the distribution of the change rate of response energy. Values of the change rate for each observation point are statistic, and it can be divided into two parts: the change rate is greater than 0.25 in the position where sand-deposit was extended to; for the rest part, the change rate should be smaller than 0.25. The black circle on Fig. 14 represents the range of sand-deposit monitored by observation window at different time.

It can be seen from Fig. 14 that the average sand-deposit radius observed by the P-wave impact imaging method agree well with the results measured by the observation window. The expanded radius of the sand-deposit measured by the P-wave impact imaging method is slightly larger than that of the observation window. The reason for this deviation is that, during the process of sand filling, the high-density flowing sand-water mixtures in the bottom of the test platform result in an increase of mass density and wave velocity of sand-deposit layer, and increase the change rate of response energy.

By comparing Fig. 15 with Fig. 13, we can see that the radius of sand deposit and interface width of adjacent sand deposit can be controlled well by using PII method. The regions of sand foundation with higher relative compactedness (≥ 0.64) have a good correspondence with the regions with high change rate (≥ 0.30). So, this method can roughly detect the distribution of higher relative compactedness of the sand-deposit. In Fig. 14(b), (c), (d) and (e), it can also be found that the change rate on the area in red circle, which increase from 0.25 to more than 0.30 in the seventh and ninth time measurement. Therefore, the relative compactedness distribution of the sand deposit is a dynamic process in the process of sand filling. So, the P-wave impact imaging method can detect the expansion of radius and the distribution of higher relative compactedness of sand-deposit in the process of sand filling.

5. Conclusions

In this paper, a full-scale model test of sand filling method in immersed tube tunnel was carried out, and P-wave impact imaging method was applied in the monitoring of the formation process of filling sand foundation. The relationship between the change rate of P-wave response energy and the radius of the sand-deposit were discussed. In this research, Kriging interpolation method was utilized to obtain the cloud map of the distribution of PII during sand filling, and the results are compared with result recorded by observation window. On basis of the above research work, the following conclusions can be draw:

(1) Through the full-scale model test, it can be found that with the progress of sand filling, the expansion rate of the sand-deposit radius first increases and then decreases. The radius of sand deposit and interface width of adjacent sand deposit can be controlled well by using PII method.
(2) When the sand-deposit contact the bottom of the test platform, the mass density and the wave velocity of sand-deposit is significantly larger than those of water, the reflection P-wave energy will decrease. So, the change rate of response energy can be used to detect sand-deposit. The threshold value of change rate can be calibrated by model test or field test. P-wave impact imaging method can detect the distribution of higher relative compactedness of sand-deposit during sand filling. Kriging interpolation principle can be used to realize a complete evaluation of the sand-deposit by calculating the cloud map of the distribution of PII.

To sum up, the method can realize the detection of spatiotemporal evolution law of sand-deposit during sand filling accurately, and provide an accurate monitoring method to control the sand filling time in the construction of Immersed tube tunnel foundation.

Acknowledgements

This work is financially supported by the National Key R&D Program of China (2018YFC0809400).

References

Chang, Y.F., Wang, C.Y., Hsieh, H., 2001. Feasibility of detecting cracks embedded in the concrete structure embedded in the concrete structure by reflection seismology method. NDT E Int. 34 (1), 34–48. https://doi.org/10.1016/S0963-8695(00)00030-X.

Chen, S.Z., Chen, Y., Zhang, M., 2002. Immersed Tube Tunnel Design and Construction. Science Press, Beijing (in Chinese).

Che, A.L., Huang, X.C., Guo, Q., Feng, S.K., 2011. Evaluation of mud-jack method filling effect of immersed tube tunnel using surface wave survey method. J. Shanghai Jiaotong Univ. 45 (5), 648–658.

Dalton, R.P., Cawley, P., Lowe, M.J.S., 2001. The potential of guided waves for monitoring large areas of metallic aircraft fuselage structure. J. Nondestr. Eval. 20, 29–46.

https://doi.org/10.1023/A:1010601829968.
Feng, S.K., Che, A.L., Wang, H., Huang, T., 2013. Study on the theory, method, and application of impact imaging method for grouting evaluation. In: Proceedings of the 11th SEGJ International Symposium; Geophysical for Establishing Sustainable Secure Society. Yokohama, 18–21, November.
Glerum, A., 1995. Developments in immersed tube tunnelling in Holland. Tunn. Undergr. Space Technol. 10 (4), 455–462. https://doi.org/10.1016/0886-7798(95)00031-S.
Gomes, L., 1991. Sydney Harbour Tunnel— structure of the Immersed tube section. Tunn. Undergr. Space Technol. 6 (2), 221–226. https://doi.org/10.1016/0886-7798(91)90069-G.
Grantz, W.C., 2001a. Immersed tube tunnel settlements-Parts 1: Nature of settlements. Tunn. Undergr. Space Technol. 16 (3), 195–201. https://doi.org/10.1016/S0886-7798(01)00039-6.
Grantz, W.C., 2001b. Immersed tube tunnel settlements-Parts 2: Case histories. Tunn. Undergr. Space Technol. 16 (3), 203–210. https://doi.org/10.1016/S0886-7798(01)00040-2.
Liu, C., Che, A.L., Feng, S.K., 2013. Propagation characteristics of elastic wave in layered medium and applications of impact imaging method. J. Shanghai Jiaotong Univ. 18 (3), 1–7. https://doi.org/10.1007/s12204-013-1424-z.
Liu, P., Tsai, C.D., Wu, T.T., 1996. Imaging of surface-breaking concrete cracks using transient elastic waves. NDT E Int. 29, 323. https://doi.org/10.1016/S0963-8695(96)00036-9.
Malhotra, V.M., Carino, N.J., 1991. CRC Handbook on Nondestructive Testing of Concrete. CRC Press, Boca Raton, FL.
Pan, Y.R., Peng, J., Naotake, Saito, 2004. Technology of sand injection for the foundation of immersed tube elements on the external ring of shanghai. Mod. Tunn.Technol. 41 (1), 41–45. https://doi.org/10.13807/j.cnki.mtt.2004.01.009. (in Chinese).
Rasmussen, N.S., 1997. Concrete immersed tube tunnels forty-years experience. Tunn. Undergr. Space Technol. 12 (1), 33–46. https://doi.org/10.1016/S0886-7798(96)00061-2.
Rose, J.L., 2002. A baseline and vision of ultrasonic guided wave inspection potential. J. Press. Vessel Technol. 124 (3), 273–282. https://doi.org/10.1115/1.1491272.
Tong, J.H., Liao, S.T., Lin, C.C., 2007. A new elastic-wave-based imaging method for scanning the defects inside the structure. IEEE Trans. Ultrason. Ferroelectr. Freq. Control 54 (1), 128–137. https://doi.org/10.1109/TUFFC.2007.218.
Tongeren, Ir., Van, H., 1978. The foundation of immersed tube tunnels. In: Delta Tunnelling Symposium. Netherlands, Amsterdam, pp.48–57.
Wei, L., Fang, Y.G., Mo, H.H., 2014. Model test of immersed tube tunnel foundation treated by sand-flow method. Tunn. Undergr. Space Technol. 40, 102–108. https://doi.org/10.1016/j.tust.2013.09.015.
Wang, G.H., Li, Z.G., Cheng, X.M., et al., 2009. Sand flowing experiment and experiment result analysis: case study on sheng wudao–daxuecheng immersed tube tunnel. Tunn. Construct. 29 (2), 176–180 (in Chinese).
Zhang, Q.H., Gao, W.P., 2003. Comparison analysis on treatment methods of pipe-sinking tunnels. Rock Soil Mech. 24 (Supp), 349–352. https://doi.org/10.16285/j.rsm.2003.s2.082. (in Chinese).